

FLIGHT PERFORMANCE AND DYNAMICS OF AN UNCONVENTIONAL SOLAR POWERED UAS

Gilbert Charruaz*a, Alessandro Borgiaa, Andrea Braghina, Tommaso Bussia, Alfredo Espositoa & Alessandro Pescosolidoa

^aDepartment of Mechanical and Aerospace Engineering, Politecnico di Torino, Corso Duca degli Abruzzi 24, Italy *Corresponding author, e-mail: gilbert.charruaz@studenti.polito.it

Abstract

The escalating concern for sustainable aviation has witnessed a substantial surge in recent years, propelled by a confluence of economic imperatives and ecological considerations. The focal point of this article is the Record Aircraft project, an autonomous Unmanned Aerial System (UAS) distinguished by its capacity for solar-powered flight. This study will delve into the flight dynamics and performance aspects of the aircraft, revealing the iterative process that resulted in the final design.

Commencing in 2017, the Record Aircraft (RA) project has undergone substantial transformations by 2023, culminating in the development of an innovative Unmanned Aircraft System (UAS) RA 2.0 with an unconventional configuration, increased size, and heightened performance. This evolution stems from the success of the initial RA FP ("Amelia") prototype, which served as a pivotal learning tool. Tests conducted with the first prototype not only validated the concept but also provided valuable insights that significantly enhanced our design, construction, collaboration, and teamwork skills. The transition to the new UAS represents a quantum leap in both technological capability and team expertise.

The mission operation of the RA 2.0 project is intricately tailored to technical specifications. Engineered for a ten-hour endurance and a 300-kilometre range, the aircraft prioritises low-speed flight to optimise energy efficiency, especially during critical phases like takeoff where power absorption is maximal. Buffer batteries are strategically incorporated to manage energy demand, ensuring both flight safety and load balancing. In the operational setup, a seamlessly adapted commercial flight computer discreetly plays a vital role in achieving precise control of the RA UAS, maintaining the most efficient flight attitude.

Keywords: UAS, Unconventional design, Aircraft performance, Sustainable aviation, Solared-powered UAS

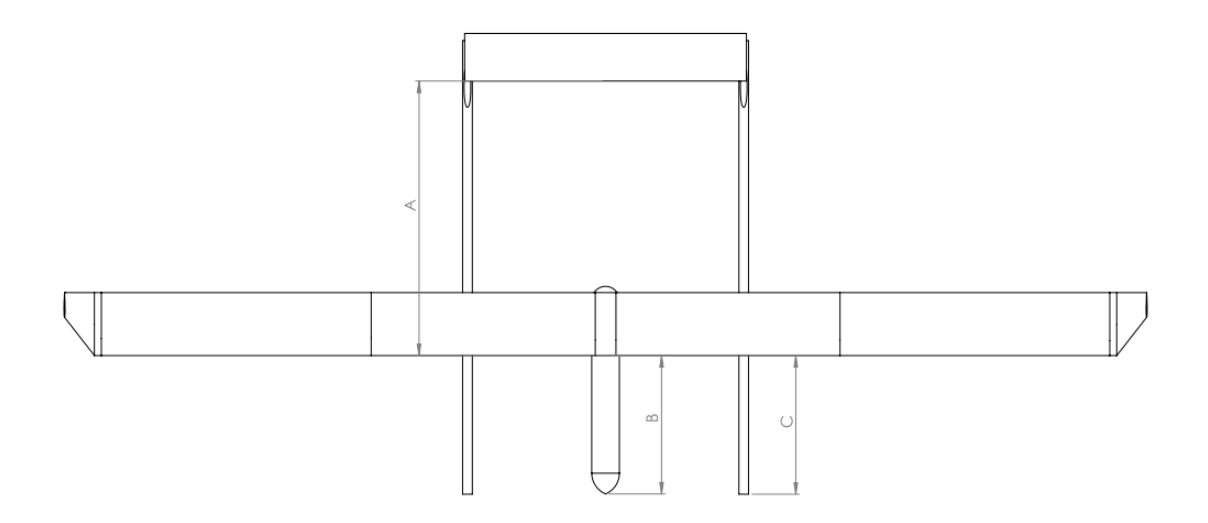


Figure 1 – Top-down projection of RA 2.0

1. Aircraft Stability Analysis

Unlike conventional aircraft designs, RA 2.0 has a higher tail-to-wing surface ratio, with the tail playing a significant role in the aircraft's total lift, contributing to approximately 15%. This design reduces drag and results in a lifting tail element. The lift distribution is chosen for stability and to minimise induced drag, considering the wing's higher aspect ratio. Due to these reasons, and the installation of solar panels over the surface, tail weight is not negligible. An analysis was carried out to determine the effect of the tail position and size on the longitudinal and latero-directional stability.

One of the main problems derived from the presence of solar panels on the tail was a center of mass positioned too far back towards the tail of the aircraft. This resulted in a not sufficient static margin, thus a reduced static and dynamic stability. To solve this problem it was decided to analyze the effect of a change in the position and size of the tail. By changing these two parameters we are affecting the position of the aerodynamic center and of the gravity center of the aircraft. A prediction on the effect can be made. Moving the tail backwards and increasing its size both move the aerodynamic center and center of gravity backwards. The total effect on the static margin however depends on the two effects combined.

On a first trial it was analyzed exclusively the influence of the tail position. It has been found that moving the plane tail backwards (distance A in Figure 1) does not increase the static margin, unlike conventional aircraft. This is because the centre of gravity moves back faster than the aircraft's neutral point does. This trend can be seen in Figure 2, where the slope of the centre of gravity points with respect to the tail position is steeper than the points representing the neutral point. The neutral point has been calculated both analytically (eq.1) and through computational approaches, using the VLM method. The computational calculations have been used in specific points to verify the analytical solution, as shown in the figure.

$$x_{n} = x_{a}^{'} + \frac{a_{t}}{a} c \bar{V} \left(1 - \frac{\partial \varepsilon}{\partial \alpha} \right) \tag{1}$$

The change in static margin in figure 2 is relative to the initial static margin as shown in the equation below:

$$\Delta(s.m.) = \frac{s.m._{new} - s.m._{old}}{s.m._{old}} \times 100 \ [\%]$$
 (2)

There is a slight benefit in advancing the tail to improve static margin, but this must be balanced against the disadvantages of loss of directional stability and consequently a need of a higher tail. The

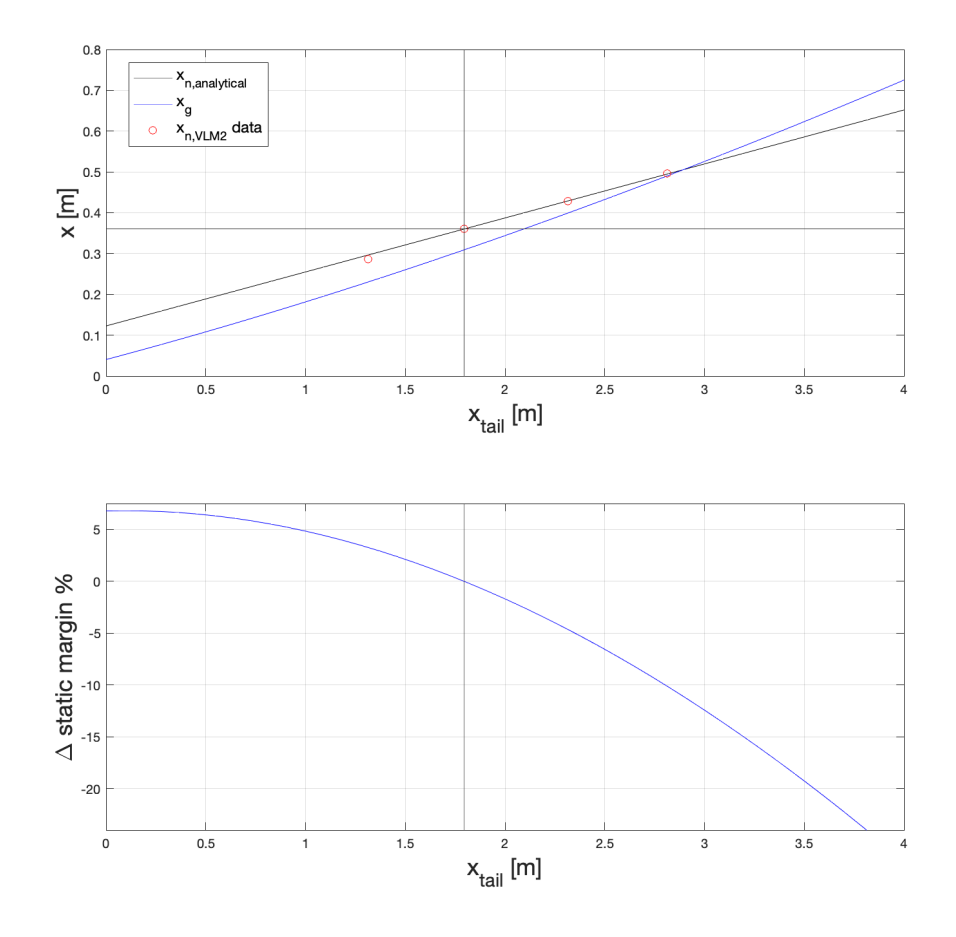


Figure 2 – Neutral point position and static margin vs. tail position

ideal distance could been chosen considering these two factors.

The need of a greater static margin has lead to a more detailed analysis where both the position and size of the tail were considered. In this analysis it was also taken in account that when changing the tail position the volume ratio \bar{V} of the vertical tail has to be kept constant. The tail has to be as small as possible and at the same time guarantee an adequate directional stability. To satisfy this two requirements a reference volume ratio was chosen in the preliminary design process and it was kept constant in this analysis. This means that when bringing the tail forward the size and weight of the vertical tail has to increase, the opposite when moving the tail backwards.

The results of this analysis are shown in two figure. Figure 3 shows the change in static margin while figure 4 shows the change in weight of the UAV.

By looking at the results we can observe that when keeping the dimension of the horizontal tail the same, the analysis confirms the results obtained earlier: by bringing the tail forward there is an increase in the static margin. The same cannot be said when the size of the tail increases. In that case the effect is opposite and the static margin decreases when bringing the tail forward.

Another important result is that the size of the tail has more effect on the static margin than the position of the tail. Three cases are considered in table 1 to show the effect of the tail size while weeping the position fixed.

The values of gain in static margin are in the range of 8÷10 % while the change when moving the tail is at max 3%.

Some considerations can be made on the change in mass shown in figure 4:

• When moving the tail backwards the dimension of the vertical stabilizer decreases, however the structure that links the tail to the wing of the aircraft increases in dimension an thus in mass.

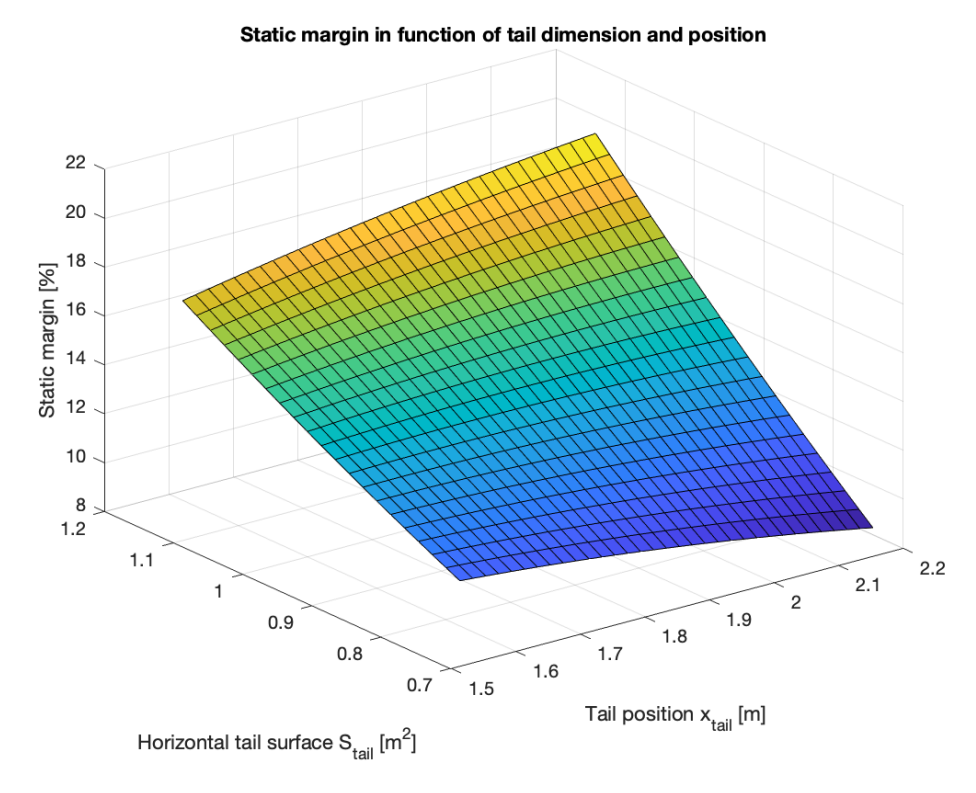


Figure 3 – Static margin in function of tail dimension and position

Tail position [m]	Tail size $[m^2]$	Static margin [% of chord]	Absolute change in s.m. [% of chord]
1.8	0.7 1.1	10.638 19.114	8.4760
2	0.7 1.1	9.831 19.780	9.9490
2.2	0.7 1.1	9.154 20.152	10.998

Table 1 – Static margin in function of tail dimension and position

This change was calculated considering the weight per length ratio *R* as constant:

$$\Delta M = R \times \Delta L \tag{3}$$

While this can be inaccurate compared to a detailed design of a structure, it can be considered appropriate for this type of the analysis.

• When increasing the span of the tail the mass increases rapidly. This happens because in addition to the structure itself, also the mass of the solar panel increases as it was decided to place solar panels on the additional surface.

1.1 Trade off analysis

A trade-off analysis was conducted to identify the optimal tail position and size. Initially, six potential configuration of tail positions and horizontal tail surface were identified.

The next step was the selection of figures of merit. The following parameters were chose among others as the most significant for the evaluation of the alternatives:

• Static margin and dynamic longitudinal stability: the acceptable static margin for the aircraft is considered to be above 14%, in accordance with the concept of static margin and dynamic

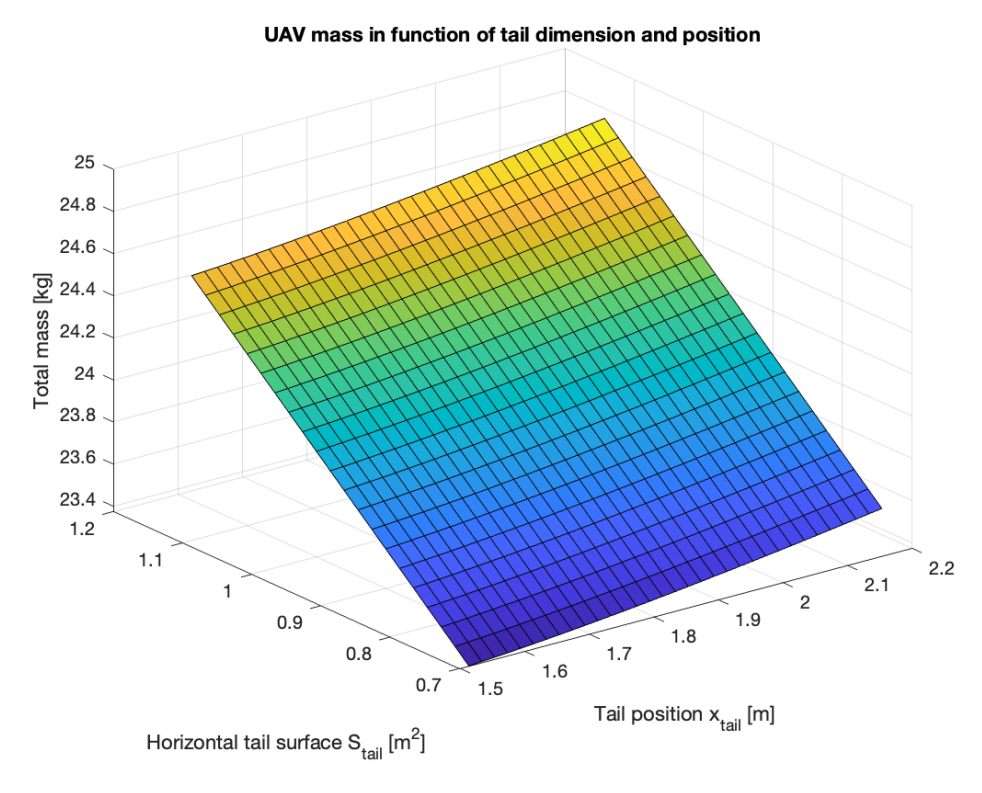


Figure 4 – UAV mass in function of tail dimension and position

	Tail position [m]	Tail size [m^2]
1	1.8	0.7
2	1.8	1.05
3	2	0.7
4	2	1.05
5	2.2	0.7
6	2.2	1.05

longitudinal stability. Such a static margin ensures the dynamic longitudinal stability of the aircraft, with an acceptable frequency for short-period and phugoid oscillations.

- Lateral stability: lateral stability is evaluated in terms of the aircraft lateral dynamics modes. In particular, the main concern for a medium-size drone is the spiral mode. Preliminary analysis of the aircraft under consideration highlights a greatly undamped spiral mode. In this analysis, which concerns the tail position and size, the directional stability is affected. It can be demonstrated that the distance between the centre of gravity and the vertical tail centre of pressure exerts a direct influence on the $C_{n\beta}$ derivative. Consequently, lateral stability, specifically the spiral mode, is analysed in this trade-off analysis in terms of directional stability $C_{n\beta}$. The goal is to guarantee that the spiral mode results in a damped or slightly non-damped mode with a period of more than 20 seconds.
- Number of solar cells: the tail and wing surfaces host the solar cells of the aircraft. A significant number of solar cells is necessary to maximize the produced power. Nevertheless, the addition of a considerable number of solar cells to the tail of an aircraft may result in a heavier tail, which could have a detrimental impact on the aircraft's static margin.

$$\frac{C_{l\beta}}{C_{n\beta}} > \frac{C_{lr}}{C_{nr}} \tag{4}$$

¹A simplified model of the spiral mode dynamic stability is

• Total aircraft mass: the relocation of the tail backwards will result in an increase in the overall weight of the aircraft due to the elongation of the aft fuselage sections. The same principle applies to the increase in the surface area of the tail.

Once the various configurations have been defined, it is necessary to compare the different figures of merit to determine the most relevant ones. To do this, the table 2 is used. The logic of the table is to take a pair of FOMs and choose the more important one.

The value 0 indicates that the FOM in the column is more relevant, while 1 indicates that the FOM in the row is more relevant. The sum of the ones in each row determines the weight to assign to the respective FOM. It was decided to increase all weights by one to ensure that complexity has a non-zero weight.

	Static margin and dynamic longitudinal stability	Lateral stability	Number of Solar cells	Total aircraft mass	Sum	Total
Static margin and dynamic longitudinal stability	/	1	1	1	3+1	4
Lateral stability	0	/	0	0	0+1	1
Number of Solar cells	0	0	/	1	1+1	2
Total aircraft mass	0	1	0	/	1+1	2

Table 2 – FOMs weight

It was concluded that is should be considered of greater importance the longitudinal static stability compared than the lateral stability. This is because the spiral mode can be successfully managed also by increasing the dihedral effect, thereby increasing the magnitude of the $C_{l\beta}$ derivative.

The fourth step was establishing a judging criteria to assign a score for each figure of merit. Each one was characterised using a range from -100 to 100. Negative values were used when an insufficient value was considered.

With regard to the static margin, the objective was to provide a benefit to the solutions with a positive difference in relation to the lower limit of 14% and to emphasise the small difference in magnitude between the solutions. In fact, a difference of 1 percentage point results in a significant difference in the flight mechanics of the aircraft. The following expression has been employed:

$$static margin score = \frac{static margin - 14}{14} * 200$$
 (5)

Therefore, solutions with a lower static margin than the acceptable value result in a negative score. Conversely, the configurations with a positive difference demonstrate a notable discrepancy in their respective scores.

A similar approach was taken to calculate the aircraft mass score. First, the weight target value of 23 kg was subtracted from the effective weight to determine the difference. This was then multiplied by a factor of 1000/23, resulting in the aircraft mass score.

$$aircraft mass score = \frac{aircraft mass - 23}{23} * 1000$$
 (6)

The number of solar cells has been assigned a score equal to the effective number of solar cells, resulting in a score of 28 and 44, respectively, for the tail of 0.7 m^2 and 1.1 m^2 .

	Static margin and dynamic longitudinal stability	Directional stability $\left(C_{n\beta}\right)$ $\left[10^{-2}\right]$	Number of Solar cells	Total aircraft mass [kg]
1	10.638	2.32753	28	23.4549
2	17.9142	2.32753	44	24.554
3	9.831	2.77669	28	23.532
4	18.3981	2.77669	44	24.6322
5	9.154	3.19605	28	23.6214
6	18.720	3.19605	44	24.721

	1) 1.8m, 0.7m ²	2) 1.8m, 1.05m ²	3) 2m, 0.7m ²	4) 2m, 1.05m ²	5) 2.2m, 0.7m ²	6) 2.2m, 1.05m ²
Static margin score	-48.02	55.91	-59.55	62.83	-69.22	67.42
Aircraft mass score	19.77	67.56	23.13	70.96	27.01	74.82
Solar cells score	28	44	28	44	28	44
Directional stability score	50	50	80	80	40	40

The score for directional stability $(C_{n_{\beta}})$ was assigned arbitrarily. In particular, the goal was finding a balance between a sufficiently high $C_{n_{\beta}}$ that guarantees directional stability without promoting an unstable spiral mode.

To summarize, the various values have been incorporated int table 3. It can be observed that each row represents a single configuration, and that the columns contain the five considered figures of merit (FOMs). In the final row the symbols '+' and '-' indicate whether the corresponding FOM represents a positive or negative characteristic for the configuration in question. For example, the longitudinal stability and solar cell numbers represent positive aspects for our project, whereas the total aircraft mass represents a characteristic that should be limited.

	Static margin and dynamic	Directional stability	Solar cells	Aircraft mass
	longitudinal stability score	score	score	score
1) 1.8m, 0.7m ²	-48.02	50	28	19.77
2) 1.8m, 1.1m ²	55.91	50	44	67.56
3) 2m, 0.7m ²	-59.55	80	28	23.13
4) 2m, 1.1m ²	62.83	80	44	70.96
5) 2.2m, 0.7m ²	-69.22	40	28	27.01
6) 2.2m, 1.1m ²	67.42	40	44	74.82
	+	+	+	-

Table 3

The final step in obtaining the optimal configuration was to calculate the trade-off indices. These indices group all considerations made thus far and indicate the configuration that best meets the previously listed figures of merit. The indices are given by a ratio, with the numerator being the sum of weights for the scores of figures of merit with a positive influence and the denominator being the sum of weights for the scores of figures of merit with a negative influence for each configuration. The trade-off index that returns the highest value will indicate the optimal configuration.

$$TO_i = \frac{K_1 \cdot \text{static margin score}_i + K_2 \cdot \text{directional stability score}_i + K_3 \cdot \text{solar cells score}_i}{K_4 \cdot \text{aircraft mass score}_i}$$
(7)

The 'i' index indicates the considered configuration, and the five constants K indicate the weights of the individual FOMs.

	1) 1.8m, 0.7m ²	2) 1.8m, 1.1m ²	3) 2m, 0.7m ²	4) 2m, 1.1m ²	5) 2.2m, 0.7m ²	6) 2.2m, 1.1m ²
Trade off index	-0.7613	3.3277	-0.9993	3.5744	-2.3117	3.2456

The winning configuration results configuration four that is characterised by a tail position of 2m from the leading edge and a surface area of $1.05m^2$.

1.2 Longitudinal Stability

Following the trade off analysis, the longitudinal and latero-directional stability of the aircraft with the new tail were analyzed. In figure 5 the adimensional eigenvalues related to the longitudinal dynamic of the aircraft can be observed. The characteristics of the short period and phugoid mode are listed in table 4;

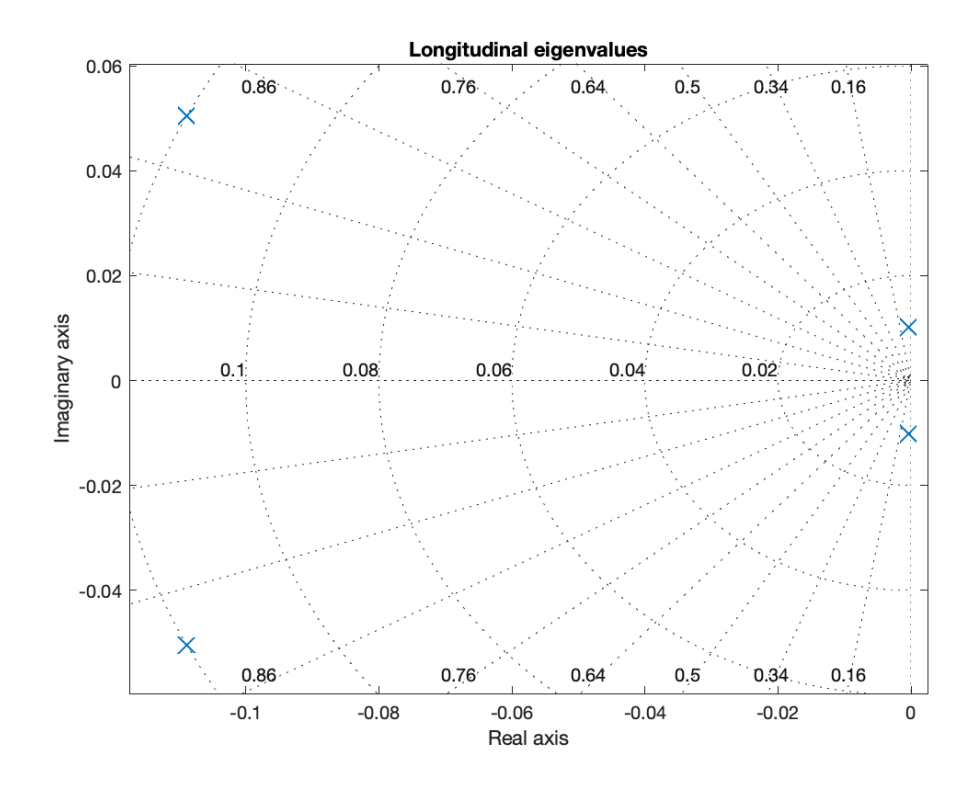


Figure 5 – Longitudinal eigenvalues (adimensional)

Mode	$\lambda [1/s]$	ω [rad/s]	f[1/s]	ζ	$t_{1/2}[s]$
Short period	$-5.4436 \pm 2.5252i$	2.5252	0.4019	0.4360	0.1273
Phugoid	$-0.0158 \pm 0.5039i$	0.5039	0.0802	0.0031	43.9060

Table 4 - Longitudinal modes

1.3 Latero-Directional Stability

The root loci of the aircraft with and without the dihedral angle can be observed in figure 6. The characteristics of the three modes are listed in two tables: 5 and 6.

Regarding lateral stability, it is important to note that although static lateral stability is ensured by $C_{l_{\beta}} < 0$ and $C_{n_{\beta}} > 0$, small to medium UAS tend to have a rather unstable spiral mode, as is the case with the studied model. An easy solution is to increase the module of the $C_{l_{\beta}}$ derivative by introducing a dihedral angle on the wing. In table 6 it can be observed that by adding a 4.5° dihedral angle the time to double of the spiral mode doubles.

Dihedral angle	$\lambda [1/s]$	ω [rad/s]	f[1/s]	ζ	$t_{1/2}[s]$
0°	$-0.3743 \pm 1.0120i$	1.0120	0.1611	0.0525	1.8518
4.5°	$-0.3231 \pm 1.0876i$	1.0876	0.1731	0.0438	2.1453

Table 5 - Dutch roll mode

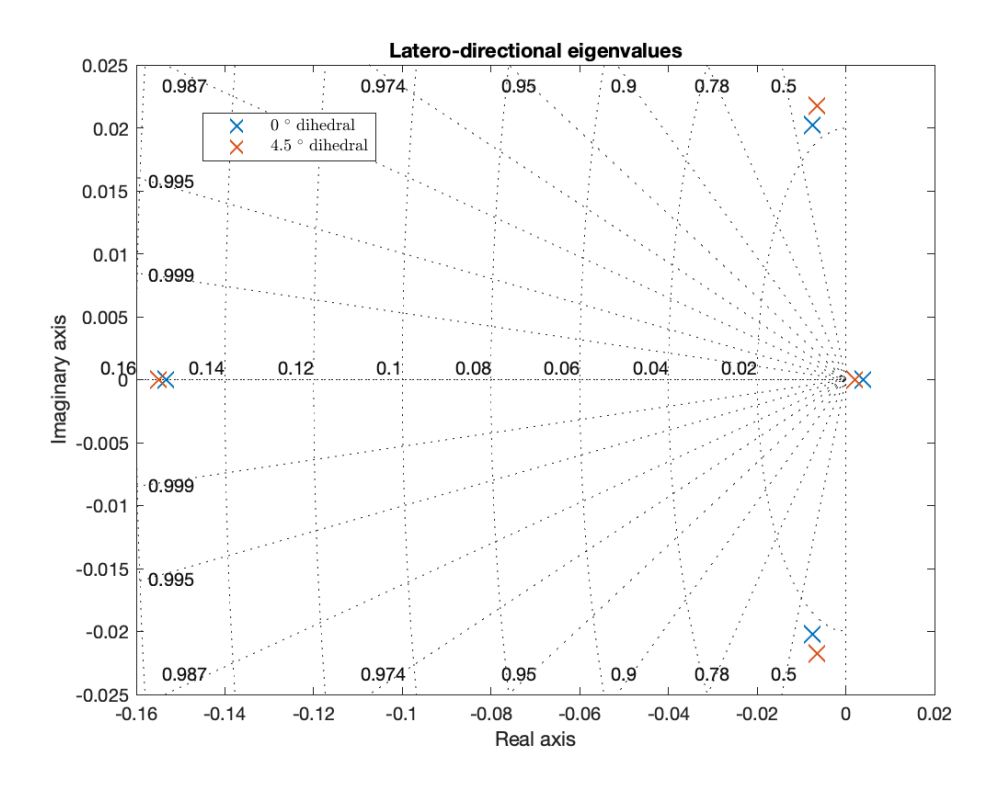


Figure 6 – Latero-directional eigenvalues (adimensional)

Dihedral angle	Time to double spiral amplitude	Roll mode $t_{1/2}$
0°	56.59 sec	1.4360 sec
4.5°	110.32 sec	1.4193 sec

Table 6 – Spiral and roll mode characteristics

2. Mass distribution

Due to the nature of the design and the propulsion mode adopted, an important percentage of the mass of the aircraft consists of batteries. However, their arrangement can be well studied, within the limits of structural and systemic feasibility, in order to obtain advantages in terms of aircraft stability. In fact, after several iterations, a particular arrangement of the batteries has been chosen. At the beginning, the batteries were organised into four packs, each containing six batteries. These packs were symmetrically positioned above the side fuselages, located at the leading edge of the wing and placed ahead of the front spar. This allowed the overall aircraft's centre of gravity to be advanced from the neutral point, but not enough to achieve a static margin of at least 15%, a design requirement. Therefore, it was decided to remove two of the eight battery packs in the wings, specifically the outermost ones, and relocate them into the central avionics bay in front of the wing. This has two main benefits: firstly, it increases the static margin towards the design value; secondly, by reducing the mass in the wings, there is less inertia to roll, which improves aircraft stability and response. Nevertheless, this repositioning introduces the potential for electromagnetic interference issues between the batteries and the overhead avionics bay. So, A new solution was developed, comprising the design of a specific case to contain the batteries directly behind each engine, in the side fuselages of the plane. This allows a strictly bonded connection between the propellers and their power supply, reducing the length and mass of the power wires. It also permits exceeding the designed static margin, allowing the distance of the engines from the leading edge of the wing to be slightly reduced. This solution is beneficial from an aerodynamic and structural standpoint, as it reduces the moments at the junction between the side fuselage and the wing, due to the forces acting on the propeller disk. Additionally, it provides a cooling system for the batteries, facilitating air intake for both the batteries and the ESC of the motor. Finally, this distribution allows for the transportation of a low-weight payload in the central bay, such as cameras for search and rescue or interrogators for experimentation of new technologies on the plane, like FBG sensing for real time structural health monitoring [1].

3. Aerodynamics performance coefficient evaluation

The power budget requires values that are extremely precise. Consequently, lift and drag are calculated using the CFD method. Siemens STAR CCM+ is an accurate CFD software that employs the finite volume method to determine the required aerodynamic coefficients by establishing a calculation environment around the mesh of the studied model. This type of analysis is slower than a VLM or panel method analysis but it is more precise. The data presented in this analysis were obtained at a fixed angle of 4 degrees, consistent with the selected angle of attack. In order to analyse the model using STAR CCM+, a preliminary mesh of the entire plane was created with Altair HyperMesh, utilising a computer-aided design (CAD) of the model. The mesh was then imported into STAR CCM+ for analysis. Subsequently, a surface mesh of the model was generated using the imposed parameters. Finally, a volume mesh was created around the model, based on the geometry of the ambient environment designed for analyzing the UAS.

In order to enhance the efficiency of the UAS, a detailed analysis was conducted on the wing twist, the tail airfoil and some innovative blended winglets. Additionally, the central tank was designed to achieve a high level of efficiency, taking into account the volume of the internal systems.

The wing twist was analysed in order to achieve a high Oswald efficiency number. This number indicates the extent to which the lift distribution of the analysed wing is analogous to that of a wing with the same aspect ratio but with an elliptical lift distribution. The greater the degree of elliptical lift distribution, the greater the efficiency of the wing. To achieve an elliptical lift distribution, the wing is twisted using two linear functions. The first function begins at a twist of 2.2° at the root and terminates at a twist of 1.5° at a distance of 1.707 metres from the root. The second function begins at a twist of -1.5° at the tip and ends at a twist of 1.5° at the root. The twist was calculated using a MATLAB script and verified through a simulation to ascertain the efficacy of this solution. The wing airfoil is the EPPLER 393, a highly efficient profile that is well-suited to the project's lift requirements. The wing in question exhibited a lift of 228.3N and a drag of 8.5N. The efficiency value is 26.9.

The efficiency study of the stabilizer was crucial to the project. Unlike other aircraft, which often use

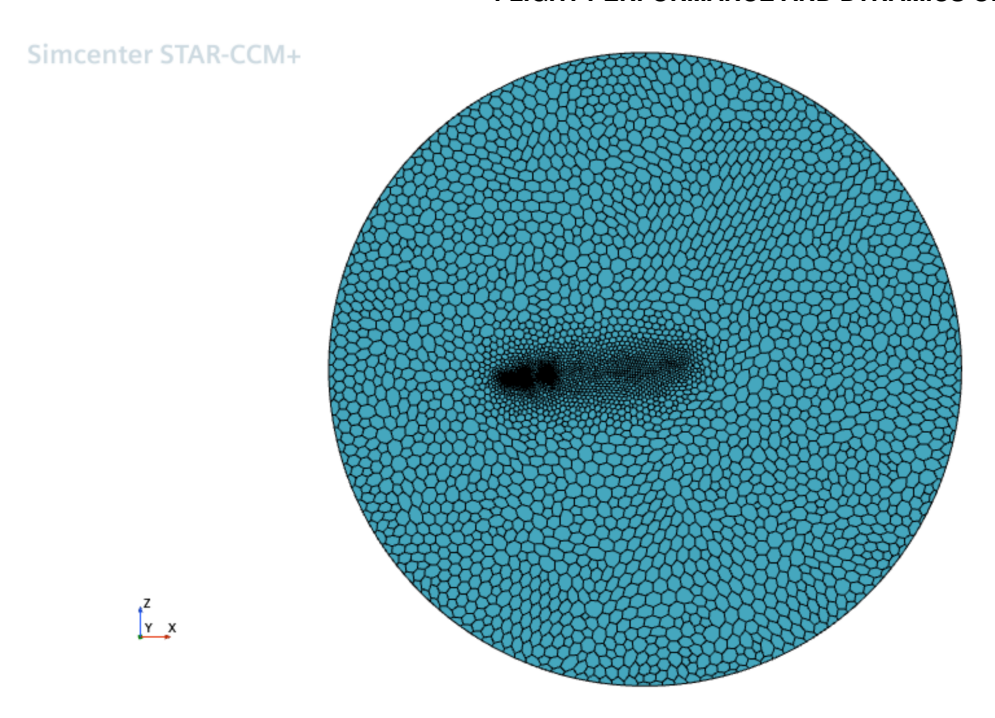


Figure 7 – Section view of the analysis ambient

downward thrust stabilizers, the tailplane in the adopted configuration generates lift, making it an unconventional design. In order to achieve this lift with the smallest possible resistance, an extensive search between a variety of airfoils was conducted. The final selection for the airfoil was the NACA 2411. Subsequently, it became evident that the plane's stability was not guaranteed, necessitating the use of a different lift to ensure stability. Therefore, a different airfoil, the Clark V, was selected. With a geometric incidence of 0 degrees of the tail, the stability of the aircraft was found to be at approximately 4 degrees of incidence. The efficiency of this airfoil is superior to that of the previous iteration. While the lift remains comparable, the drag is significantly reduced. Furthermore, the benefits of this airfoil extend to the systems integration. The enhanced thickness of this airfoil allows the electromechanical actuators to be placed inside the tailplane, improving the mass distribution and the design for ease of construction. A comparison of the two models revealed that the CLARK V-equipped model exhibited an enhanced efficiency of 1% relative to the NACA 2411 airfoil-equipped model.

In order to enhance the efficiency of the winglets, a comparative analysis of various models was conducted. A thorough review of theses and research papers was carried out to determine the most suitable type of winglet for our project. The blended winglet was selected as the optimal model, although there is no specific information available regarding its design. Consequently, a list of different parameters was created for editing. The sweep angle, cant angle, chord and length were all subject to change. Additionally, two distinct airfoils were tested: the NACA 0008, a symmetrical airfoil, and the PSU 94097, an asymmetrical airfoil employed on sailplane winglets. Another approach was to consider a point-ending winglet style. Additionally, the curvature of the leading edge of the winglets was modified in order to ascertain whether there were any discernible differences. While the full analysis is not yet complete, preliminary results indicate that the wing efficiency has improved by approximately 3%. One limitation of the winglet design is that it cannot be made too high, as this would cast a shadow on the solar panels mounted on the wing. Additionally, the potential benefits of incorporating downward-facing winglets on the tailplane is being investigated, with the objective of further enhancing the overall efficiency.

The following table presents the results of the analysis that has already been conducted. A comparison of the data from the table indicates that the most efficient winglet configuration is currently the model with a length of 230mm, a tip chord of 230mm, a cant of 30°, a sweep of 45° and the NACA 0008 airfoil.

The central tank was designed to accommodate all the UAS systems. This component represents the

Length	Winglet tip chord	Cant [deg]	Sweep [deg]	Airfoil	Cl	Cd	Efficiency	Delta efficiency
	WING WI	THOUT WII	NGLET		0,839	0,0312	26,89103	
230	230	15	45	PSU	0,886	0,0321	27,60125	2,6411059
230	230	30	45	PSU	0,885	0,0321	27,57009	2,525258151
230	230	45	45	PSU	0,886	0,0322	27,51553	2,322344702
230	230	30	45	NACA	0,884	0,0318	27,79874	3,375536915
230	230	45	45	NACA	0,891	0,0321	27,75701	3,220344647
230	230	30	30	PSU	0,896	0,0323	27,73994	3,156861515
	POINT MODEL				0,88	0,0317	27,76025	3,232404507

Figure 8 – Winglet analysis

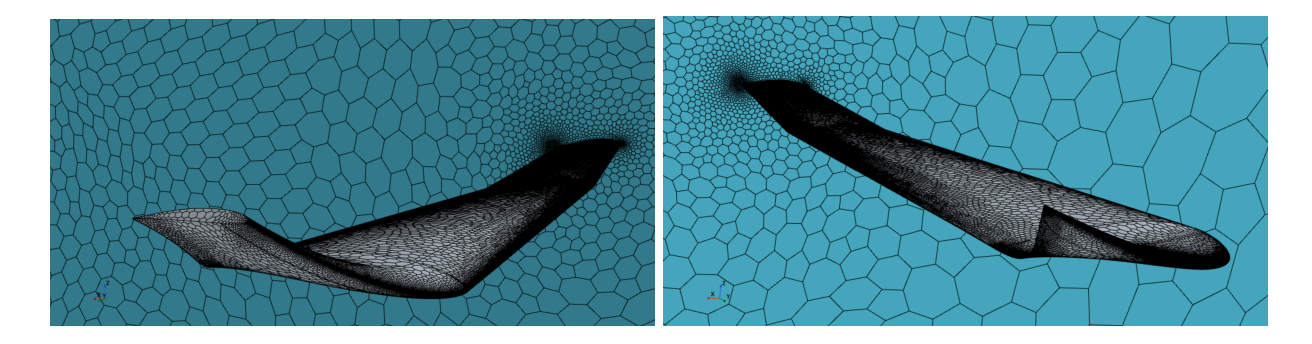


Figure 9 – (a) Example of PSU 94097 airfoil winglet (b) Example of point-ending style winglet

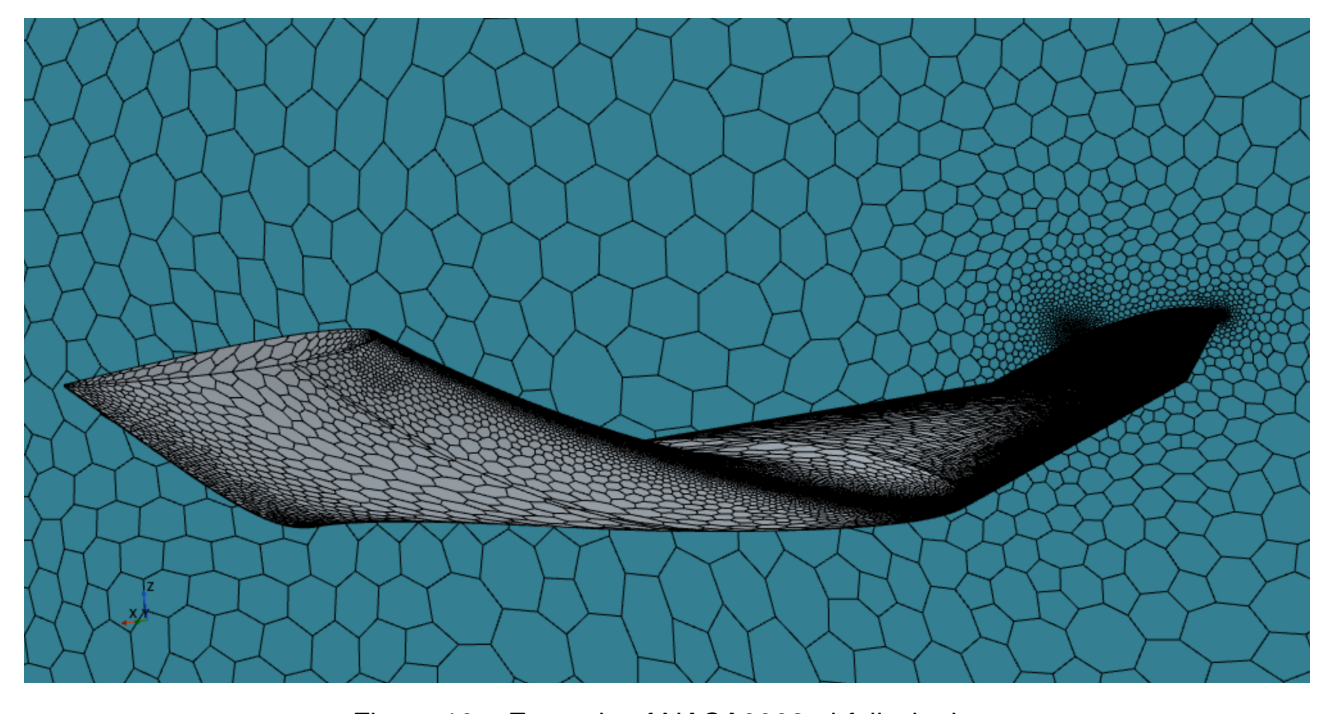


Figure 10 – Example of NACA0008 airfoil winglet

largest cross-sectional area of the aircraft when viewed from the front, and consequently, it generates a considerable amount of drag. In order to enhance the efficiency of the system, the tank was designed with a more aerodynamic shape.

Additionally, all the connections between the lateral fuselages and the central tank to the wing have been designed to be as efficient as possible, with the objective of redirecting the air in the smoothest way possible. To date, only one analysis of the entire UAS has been conducted using STAR CCM+. The model under analysis incorporates a twist in the wing and a new airfoil for the tailplane. It is anticipated that winglets and a more aerodynamic central avionics bay will be implemented in future models. The total lift of the analysed model was found to be 249.6N, while the total drag was calculated to be 12.5N. The overall efficiency of the UAS is approximately 20.

4. Stability derivatives evaluation

At the early stages of the design process, numerous analyses were conducted in order to make preliminary decisions on the main general characteristics of the aircraft, with the objective of defining its geometry and mass distribution. Among these characteristics, the effects of possible dihedral and swept angles were analysed, as well as the presence of geometric twist, in addition to the choice of the most suitable wing and tail profiles under the assumed flight conditions. The keys to this phase of the project were therefore twofold: speed of calculation and reliability of the results. Following a meticulous examination of the available options, the decision was made to utilise OpenVSP (Open Vehicle Sketchpad), a parametric aircraft geometry tool developed by NASA. OpenVSP enables users to create three-dimensional aircraft models and perform engineering and aerodynamic analyses on these models, allowing the attitude and configuration of the aircraft to be easily modified and reducing the cost of the calculations. OpenVSP provides a range of geometries commonly used in aircraft modelling, including wings, pods, fuselages, and propellers, which can be modified and assembled into a complete aircraft model. Following the addition of each geometry, the software enables complete customisation via a straightforward and concise interface. It is possible to modify the more general characteristics of each component, such as their position in space, geometry, and material. Ultimately, the objective is to refine the mesh generated by the program to enhance the reliability of the analysis. OpenVSP offers a range of tools for conducting structural and aerodynamic analyses. In this instance, the VSPAERO environment was selected, a thin-surface code for inviscid subsonic and supersonic aerodynamics. This code is capable of calculating the aerodynamic loads acting on the aircraft (lift, drag and momentum), as well as all the derivatives necessary to analyse the stability of longitudinal and lateral-directional motions. The next step was to select a method for analysis from the two proposed in VSPAERO: the Panel Method and the Vortex Lattice Method (VLM). Both the VLM and Panel methods are linearised aerodynamic tools based on potential theory. VSPAERO currently operates in two modes: the mean surface approach (commonly referred to as VLM) and the wetted surface approach (referred to as the Panel method). In the mean surface approach, lifting surfaces such as wings and rotors/helices are represented by their mean camber surfaces, composed of discrete vortices, in order to calculate parameters such as lift, induced drag, lift curve slope and lift distribution. If the airfoils are curved, these surfaces exhibit curvature. These surfaces exist in threedimensional space and capture the three-dimensional effects of flow. They generate wakes and can support forces and moments. Non-lifting bodies, such as fuselages and pods, are represented in three dimensions by two mean surfaces arranged in the shape of a cross. These surfaces, which may be flat, exist in three-dimensional space and capture the effects of three-dimensional flow. However, they do not generate wakes or support forces. Nevertheless, they can support moments and influence forces on neighbouring lifting surfaces. It is important to note that the method does not take into account the influence of model thickness and fluid viscosity, thus precluding the calculation of viscous resistance. In contrast, the wetted surface approach (Panel Method) is based on the principle of overlaying surface distributions of aerodynamic solutions across small quadrilateral sections (panels) of the aircraft's surface. Consequently, this method enables the accurate description of the aircraft's geometry, with no limitations on thickness [2]. Although the Panel Method may appear to be a more accurate and reliable approach than the VLM, the latter is an effective method for lifting surfaces. It requires less than half the number of panels typically used, which results in a significant reduction in computational cost. Furthermore, it avoids the common issues encountered with wingtips and trailing

edges. In contrast, the Panel Method did not show consistency in its results. It proved to be less accurate than the VLM in some cases when compared to CFD data. The optimal approach would have been a hybrid mode in which lifting surfaces were modelled with the Vortex Lattice Method (VLM) approach and non-lifting surfaces with the Panel Method. These multiple reasons led to the selection of the VLM as the primary method for preliminary aircraft analysis.

One possible analysis of the Vortex Lattice Method was employed to study the static stability of the aircraft, the STEADY mode. Other analyses are more useful for studying a dynamic response of the system, which generates sinusoidal components in the motions of roll (p), pitch (q) and yaw (r) to analyse the unsteady derivatives of the aircraft. Conversely, the steady analysis, conducted at a predefined geometric angle of incidence, calculated each aerodynamic derivatives, which proved useful for analysing the aircraft's longitudinal and lateral stability under static conditions, as well as an estimate of the neutral point. The initial concept was to design an unconventional aircraft with lifting wing and tail surfaces that could accommodate as many solar cells as possible, lightweight fuselages to support the structure, and a central tank containing various systems and a parachute. In order to enhance the reliability of the results, it was initially necessary to optimise the mesh on VSP, in order to create as few contrasts as possible within the programme. An attempt was made to have cells as square as possible, without one dimension prevailing over the other, and cells were thickened in the vicinity of the central tank and wing tips. VSP allows for complete customisation of the mesh, with the numbers of tessellated curves in the x and y directions able to be modified in order to create a dense and regular mesh. The cluster tool is also employed to thicken the mesh in certain areas. However, once the simulation was launched via VLM, the geometry that was analysed according to the aforementioned criteria was as follows (fig.11).

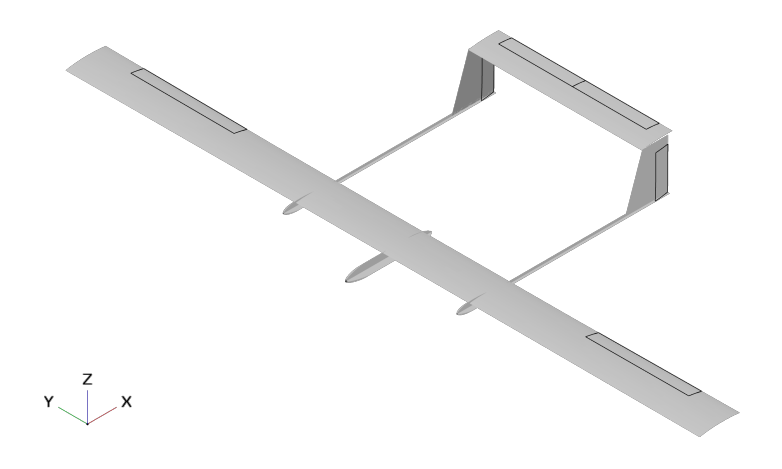


Figure 11 – VLM model analysed

The VLM model represents the initial concept of the aircraft, with a length of 1.13m and both fuse-lages that extend approximately 10cm from the wing leading edge. The initial analysis revealed two significant issues: the reduced static margin and the reduced doubling time of the aircraft's spiral mode (modelled as in section 1.3).

With regard to the static margin, the lack of a conventional configuration and the absence of a defined distribution of masses, particularly the carbon fibre panels on the aircraft, make it challenging to provide a precise estimation. Based on preliminary analyses, an anticipated minimum static margin value of 15% was selected. From the VSP simulations, it was found that this static margin could be achieved by advancing the fuselage further beyond the leading edge of the wing and changing the dimensions of the central tank. However, it will be possible to adjust this static margin as required through the distribution of the aircraft's various systems (especially batteries and cables) at a later stage. With regard to spiral mode, the initial doubling time was found to be so short that it would have led the control system to consume excessive energy in flight in order to stabilise the aircraft. The so-

lution proposed was to insert a dihedral angle from the second wing box and to reduce the size of the drifts. By varying these two characteristics, the most important derivatives of the lateral-directional dynamics, the $C_{L\beta}$ and the $C_{N\beta}$, were modified, increasing the doubling time of the spiral mode and improving the directional stability of the aircraft. Following various analyses and hypotheses, the current configuration was developed to address precisely these two problems.

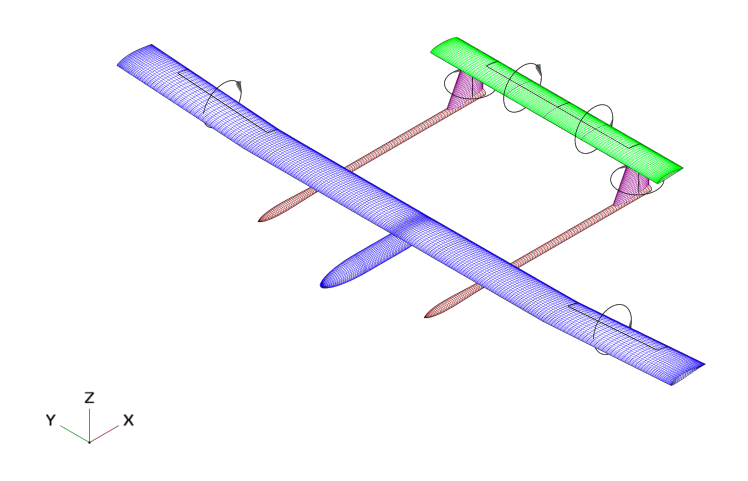


Figure 12 – VSP current model

4.1 Longitudinal Dynamics Analysis

Currently the model shows a positive dihedral angle of 4 and each drift has been reduced from 1.13m to 0.75m. Two stability analyses were then performed with the same centre of gravity coordinates $X_{ref} = 0.360m$ to evaluate the differences in terms of static margin. These analyses allowed the flight conditions to be selected: a speed of $V_{inf} = 11.5m/s$ and a reference Mach of $M_{inf} = 0.0335$ were set. Everything was analysed at a geometric angle of incidence between the wind direction and the horizontal equal to $\alpha = 4$. The next step was to select the reference surfaces for dimensioning the aerodynamic derivatives. The dimensions of the wing were chosen:

$$S_{ref} = 3.376m^2$$
 $b_{ref} = 7.34m$ $c_{ref} = 0.46m$

The VSPAERO environment analyses the system according to a user-definable number of wake iterations. After some evaluation, 8 was chosen as the minimum number of iterations to bring the simulation to convergence. At this point, the programme calculates the aerodynamic derivatives 7 times with 8 iterations. Once this is done, VSPAERO simulates the environment three more times to calculate the control derivatives of the three control surfaces implemented in the software: ailerons, elevator and rudder. The basic result of the analysis is a .stab file containing all the basic aerodynamic derivatives and an estimate of the neutral point. Once the two analyses have been completed, the first thing to check is the convergence of both. Using the current configuration as an example, it can be seen that indeed after only 8 iterations the residuals reach sufficiently low values. The figure 13 illustrates the residuals of C_l , $C_{d,tot}$ and C_{my} (the momentum coefficient around the y-axis) in the tenth and final analysis conducted by VSPAERO as the 8 iterations progress. The total drag coefficient, $C_{d,tot}$, represents the sum of the induced drag, C_{di} , and an estimate of the parasitic drag. The latter is not calculable by VSP, as the inviscid flow model it analyses does not permit such calculations.

Once the convergence of the residuals has been checked, the *.stab* file is opened and the differences on the static margins are evaluated. VSPAERO returns the coordinate of the neutral point X_{np} dimensional, but also directly the static margin SM dimensionless.

The current configuration respects the predictions made in the design phase and gives a static margin value of about 17%. On the other hand, the analysis of the initial configuration of the aircraft shows the longitudinal instability of the aircraft. In fact, the static margin is negative, approximately

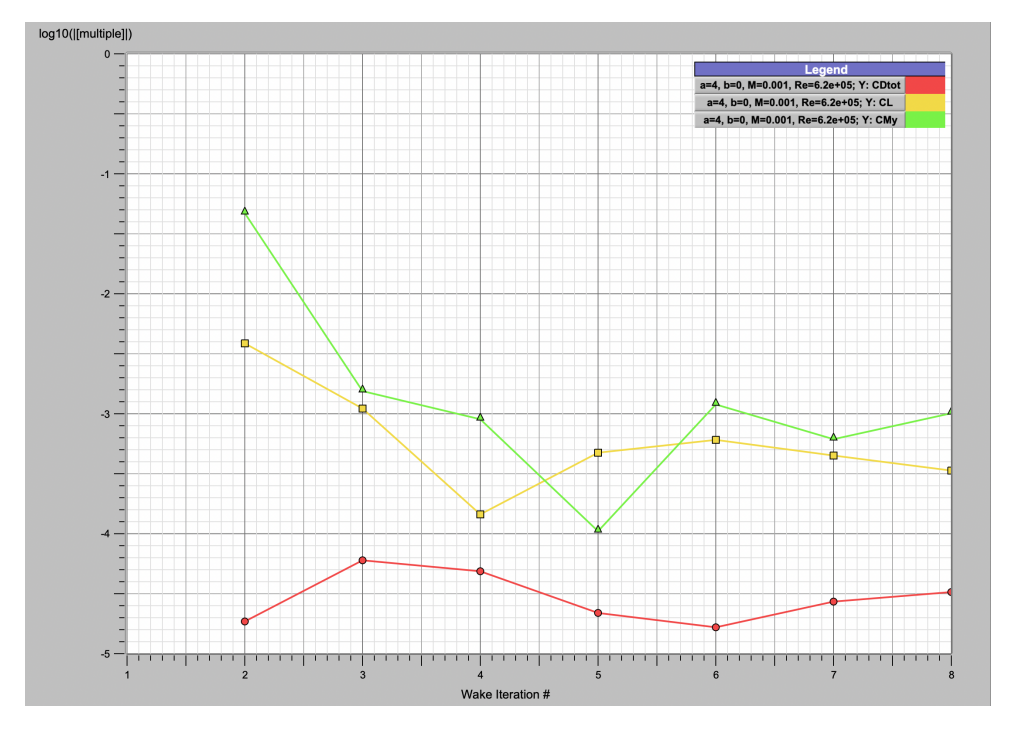


Figure 13 - Residuals stability analysis current model

	First Configuration	Last Configuration
$C_{m,\alpha}$	0.4163	-1.037
X_{np} [m]	0.3260	0.4387
SM	-0.07385	0.1712

Table 7 – Stability analysis between the two configurations with the same centre of gravity $X_{ref} = 0.36m$

-7%, showing that the neutral point is in front of the centre of gravity and that the configuration was destabilising for the aircraft.

4.2 Lateral-Directional-Dynamics Analysis

In order to evaluate the differences between the two configurations in terms of lateral-directional dynamics, two stability analyses were conducted, varying only the dihedral angle and the dimensions of the drifts. The objective was to analyse the two most important derivatives of the lateral-directional dynamics, the $C_{L\beta}$ and the $C_{N\beta}$. Prior to this, it is necessary to gain a deeper understanding of the conventions employed by VSP in the .stab output file. In general, VSP adheres to a body reference system, as illustrated in the preceding models: the x axis is oriented from nose to tail, while the z axis is oriented downwards. This reference system is utilised by VSP to calculate the moment coefficients, which are displayed in the output file as C_{Mx} , C_{My} and C_{Mz} . However, there are also moment coefficients in the .stab file that follow more conventional aviation sign conventions, denoted as C_{Ml} , C_{Mm} and C_{Mn} , which will be referred to as C_L , C_M and C_N for convenience. The $C_{L\beta}$ represents the coefficient of the momentum around the x-axis caused by a non-zero sideslip angle β . It is among the most important derivatives in sideslip analysis, and is influenced by many parameters in the aircraft configuration, but especially by the presence of a dihedral angle. In the presence of a dihedral angle, there is a difference in incidence between the two wings. To illustrate this, consider a crosswind inclined at an angle β coming from the pilot's right. The dihedral causes an increase in incidence on the right wing and a decrease on the left wing. This results in a negative stabilising roll moment (with x-axis tail to nose), which then determines the sign of the corresponding derivative. This is of great importance due to the significant influence it has on the modes of lateral-directional motion, in particular the Spiral Mode and the Dutch Roll.

The $C_{N\beta}$ represents the coefficient of the moment about the z-axis, which is always caused by a non-zero sideslip angle β . It is the derivative representing the directional stability of the aircraft, analogous

to $C_{m\alpha}$ in longitudinal stability. It is important that it be positive, as this ensures the configuration is stable in lateral-directional motion. It is slightly influenced by the fuselage, but mainly by the drifts. Assuming that the dihedral angle and the drifts are the only components of the aircraft that influence these derivatives individually, two further stability analyses were conducted on the current configuration. The first analysis eliminated the dihedral, while the second increased the size of the drifts in order to determine the changes in $C_{L\beta}$ and $C_{N\beta}$, respectively.

	with dihedral	without dihedral	Δ%
$C_{L\beta}$	-0.05351	-0.004623	-91.36%
$C_{N\beta}$	0.02514	0.03349	33.22%
SM	0.1712	0.1646	-3.851 %

Table 8 – Dihedral influence on aerodynamic derivatives

The table above illustrates the impact of dihedral on the aerodynamic derivatives. It can first be observed that the derivatives exhibit consistency in their signs across the two cases under consideration. Consequently, the presence or absence of the dihedral does not affect the anticipated behaviour of the aircraft with a non-zero sideslip angle β . However, as anticipated, the removal of the dihedral from the second wing box results in a reduction of the modulus of $C_{L\beta}$ by over 90%, while simultaneously increasing the modulus of $C_{M\beta}$ by 33%. This outcome is contrary to the findings presented in the aforementioned chapter, which indicates that such a result is highly unfavourable. In order to increase the doubling time of the spiral mode, it would be beneficial to increase the modulus of $C_{L\beta}$ and reduce it by $C_{N\beta}$. Conversely, removing the dihedral has the opposite effect, making the spiral mode doubling time very low and reducing the aircraft's ability to stabilise in flight. Furthermore, a slight variation in the static margin was to be expected, due to the differing positions of the aerodynamic centres of the wing, which resulted in a slight change to the neutral point. However, this variation had minimal impact on the study of longitudinal dynamics. The current model was analysed with the dihedral, while the drifts were extended to their original dimensions in order to assess their influence on $C_{N\beta}$.

	short drift (0.75 m)	long drift (1.13 m)	Δ %
$C_{L\beta}$	-0.05351	-0.06098	13.95%
$C_{N\beta}$	0.02514	0.06137	144,12%
SM	0.1712	0.1843	7.655 %

Table 9 – Influence of drift length on aerodynamic derivatives

As anticipated, and in accordance with the dihedral influence analysis, the magnitude of $C_{L\beta}$ is modestly influenced by the size of the drifts, exhibiting an increase in modulus of approximately 14% while maintaining its sign. Conversely, an increase in the size of the drifts by approximately 33% led to a significant increase of 144% in the magnitude of $C_{N\beta}$. Although the slight increase in modulus of $C_{L\beta}$ is beneficial in terms of the aircraft's lateral-directional modes, the large increase in $C_{N\beta}$ is highly detrimental, resulting in a significant reduction in the period of both Spiral Mode and Dutch Roll. It should be noted that even within this analysis there is a slight variation in static margin, which is of minimal consequence for calculation purposes.

5. Power Budget

The project's objective naturally revolves around a power budget within which it must operate. Indeed, being energetically autonomous comes with the obligation to always stay within certain power limits. There are no degrees of freedom, and everything is interconnected according to necessarily binding relationships, which are based on respecting the limits of the energy balance. If a certain mass is considered, a specific lift is required, thus a particular speed, and consequently, a certain thrust limited by the energy the panels can produce, which cannot be exceeded. Striking a balance among all these factors means defining a conceptually isostatic complex mechanism that leaves little room for standard solutions. Innovation lies in redefining new parameters, anticipating new scenarios, and

solving new problems. The Figure 14 clearly is the result of the interconnection between the project main variables. The process is iterative and considers a multitude of data and variables, from which a range of potential solutions can be derived. However, few of these align with the project requirements. The two fundamental inputs to the power budget are the plane aerodynamic polar and the solar panels' specific power produced $P_{sp,prod}$, which is calculated by averaging over daylight hours in a specific season.

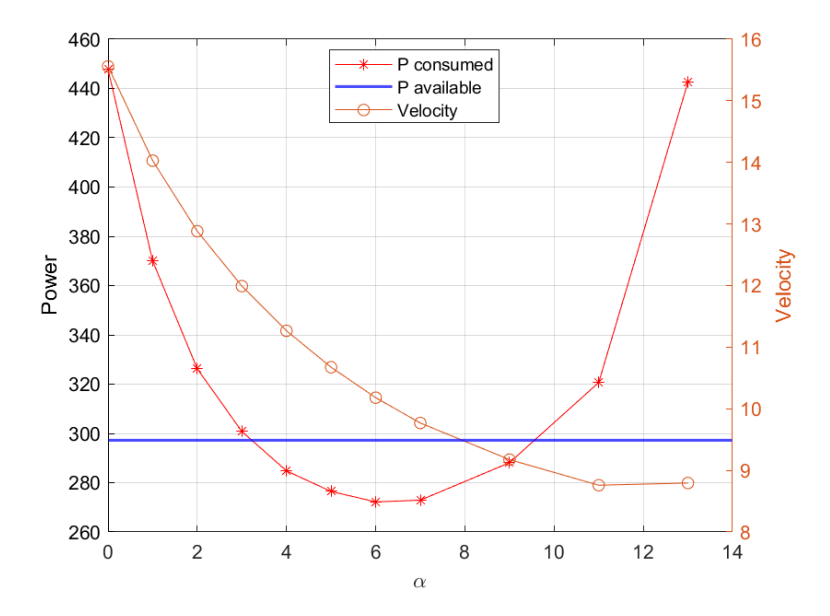


Figure 14 – Identification of flight incidence and velocity

In order to obtain a $P_{sp,prod}$ value, it is first necessary to consider the aircraft's mission and analyse it to derive the latitude and longitude. In addition, the number of hours spent in day and night flight must be specified. The mission of RA 2.0 consists of a flight in May for 10 hours during the day between 07:30 and 17:30 in the Taranto area. To obtain reliable data on the average irradiance as a function of geographical location, the European 'PHOTOVOLTAIC GEOGRAPHICAL INFORMATION SYSTEM' [3] was used, i.e. a database indicating the daily global irradiance from a statistical average of fifteen years. In addition, for practical feedback, irradiance measurements were taken using special measuring instruments on clear days in April, near Turin. The data obtained is higher than that provided by the European portal, as the latter also averages for cloudy days. Therefore, the values taken from the European database are conservative when referring to optimal mission conditions.

• Statistical Specific Power P_{sp, stat}:

Represents the average aforementioned irradiance available during the mission's flight hours, expressed in $\frac{W}{m^2}$. It can be a mean, minimum, or maximum value of irradiance during the mission.

• Panel Efficiency η_{panels} :

Defined as the efficiency with which the solar panels convert irradiance into electrical power. Provided by the manufacturer. In this specific case, it is 0.21.

• MPPT Efficiency η_{MPPT} :

Represents the efficiency of the Maximum Power Point Tracking (MPPT) system. It's an estimate because the component might be internally developed. Here, it is 0.95.

• System Efficiency η_{losses} :

Accounts for losses in the system due to soldering, cabling, connectors, and heat dissipation. Assumed to be 0.95.

• Junction Efficiency η_{junction} :

Considers the efficiency derived from the actual area of the cells considering the junctions. Determined by the ratio of the cell area without junctions to the total cell area. Here, it is 0.97.

The formula to calculate the produced specific power is:

$$P_{ ext{sp, prod}}\left[rac{W}{m^2}
ight] = P_{ ext{sp, stat}}\left[rac{W}{m^2}
ight] imes \eta_{ ext{panels}} imes \eta_{ ext{MPPT}} imes \eta_{ ext{losses}} imes \eta_{ ext{junction}}$$

These calculations take into account the combined efficiencies of the various components of the photovoltaic system, providing an estimate of the power produced for different irradiance conditions during the mission. The specific power value used for the subsequent analysis is the average of the minimum and mean value of $P_{sp,prod}$, to be conservative.

Subsequently, all other design values are considered, including mass and the number of solar cells. Next, the efficiency of the motor and propeller, along with a drag power increase factor of approximately 1.3, were considered. The specific consumption of onboard systems during cruise flight was then evaluated. Consequently, the power budget can be described as a simple differential equation in time that incorporates the aforementioned considerations and variables.

$$\frac{dE_{bat}}{dt} \approx (P_{solar} - P_{out}) \tag{8}$$

The energy linked to the state of charge (SoC) of the batteries is denoted by E, while the power produced by the solar cells is represented by P_{solar} . The total power consumed by the propellers and the onboard systems is given by P_{out} . The Figure 15 depicts the average daily irradiance trend and SoC of the batteries during daytime flight hours (quite similar to ETH Atlantik Solar analysis for this kind of operations [4]). So, it is possible to write that:

$$P_{out} = P_{motor} + P_{systems} \tag{9}$$

$$P_{solar} = P_{sp,prod} \times S_{panels} \tag{10}$$

With regard to the motor, the power consumed is dependent on an efficiency term η_{prop} that incorporates the propeller, motor, and motor-control efficiencies (it is about 0.64). Therefore, it is necessary to evaluate the consideration of the aerodynamic drag, which is multiplied by the free stream velocity to yield the required power to fly. From this, it is possible to obtain the power that must be pursued to the electrical motor P_{motor} , as was previously discussed.

$$P_{motor} = \frac{P_{drag}}{\eta_{prop}} \tag{11}$$

In the equation, the P_{drag} term incorporates a drag increase factor of 1.3, which allows for sufficient margin. All the previous terms are then used to initiate the iterative process of identifying flight configurations in which (8) value is equal or higher than zero, and to find out the right cruise flight incidence and velocity, by Figure 14.

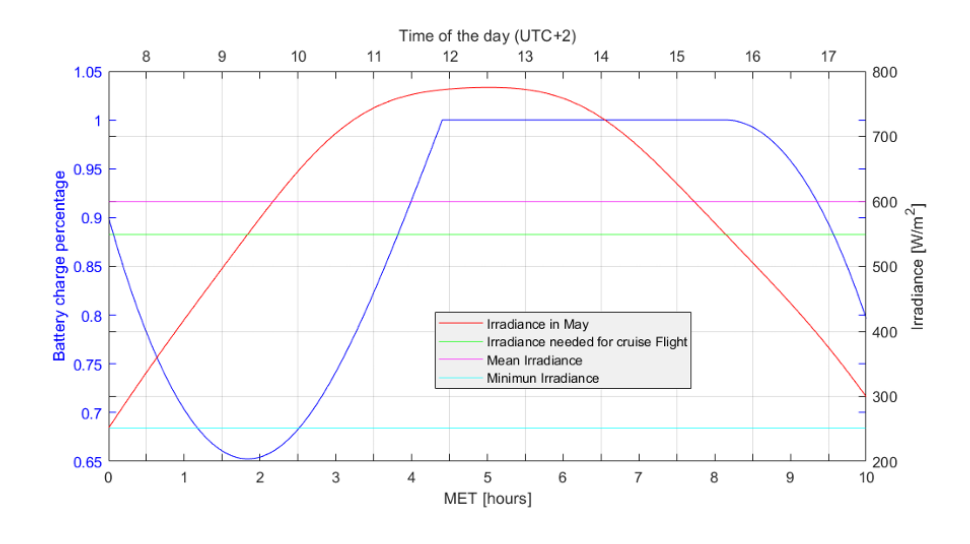


Figure 15 – Batteries percentage and irradiance (with a battery of 740Wh)

References

- [1] A. C. Marceddu, G. Quattrocchi, A. Aimasso, E. Giusto, L. Baldo, M. G. Vakili, M. D. L. D. Vedova, B. Montrucchio, and P. Maggiore, "Air-to-ground transmission and near real-time visualization of fbg sensor data via cloud database," *IEEE Sensors Journal*, vol. 23, no. 2, p. 1613 1622, 2023. Cited by: 6; All Open Access, Hybrid Gold Open Access.
- [2] F. Mariën, "Software testing: Vspaero. master thesis," Master's thesis, Hamburg: Aircraft Design and Systems Group (AERO), Department of Automotive and Aeronautical Engineering, Hamburg University of Applied Sciences, 2021.
- [3] European Commission Photovoltaic Geographical Information System, https://re.jrc.ec.europa.eu/pvg_tools/en/.
- [4] P. Oettershagen, A. Melzer, T. Mantel, K. Rudin, T. Stastny, B. Wawrzacz, T. Hinzmann, S. Leutenegger, K. Alexis, and R. Siegwart, "Design of small hand-launched solar-powered uavs: From concept study to a multi-day world endurance record flight," *Journal of Field Robotics*, vol. 34, no. 7, pp. 1352–1377, 2017.

Copyright Statement The authors confirm that they, and/or their company or organization, hold copyright on all of the original material included in this paper. The authors also confirm that they have obtained permission, from the copyright holder of any third party material included in this paper, to publish it as part of their paper. The authors confirm that they give permission, or have obtained permission from the copyright holder of this paper, for the publication and distribution of this paper as part of the ICAS proceedings or as individual off-prints from the proceedings.